Contact stresses associated with the wedge-lock mechanism in a prototype subsea pipeline recovery tool

Contact stresses associated with the wedge-lock mechanism in a prototype subsea pipeline recovery tool

Y Xing[1], N B Eriksson[1,2], M C Ong[1] and C Knutsen[2]

[1]Department of Mechanical and Structural Engineering and Material Science, University of Stavanger, Kjell Arholmsgate 41, 4036 Stavanger, Norway
[2]IK-Norway, Christian August Thorings veg 9, 4033 Stavanger, Norway

Corresponding author: yihan.xing@uis.no

Abstract. This paper examines the contact stresses associated with the wedge-lock mechanism in a prototype subsea pipeline recovery tool (PRT) through numerical methods and experimental testing. The prototype PRT studied combines IK-Norway subsea plug technology in a subsea PRT. This allows the PRT to seal the subsea pipeline while it is being retrieved. The PRT can then flush the pipeline before retrieval and therefore providing for operational cost savings. This paper presents the first stage of the study which the sealing mechanism is not studied. The current wedge-lock mechanism uses a cone to press steel balls against the insides of the subsea pipeline thereby locking the PRT to the pipeline. Designing for sufficient contact stresses is critical to ensure that the PRT can grab the subsea pipeline tightly in order to ensure a successful recovery. The contact pressure distribution between the ball and cone in the wedge-lock mechanism is modelled using finite element method in Ansys. The resulting indentation depths occurring at the pipeline are compared against physical tests. It was found that the contact problem associated with the wedge-lock mechanism is complex and the actual contact stress/final gripping force is sensitive to the input parameters. Second, the results show that the Ansys numerical model is able to represent the contract stresses fairly accurately if the friction coefficient is well-controlled. Third, it was observed that a low friction coefficient ensures low indentation depths. Last, the results highlight that an increase in the cone-angle leads to a decrease in the indentation depth.

1. Introduction and background

Pipeline recovery tools (PRTs) are used for the retrieval of subsea pipelines. During the next years, the decommissioning market for offshore and subsea pipeline is projected to grow significantly [1]. The reason is that many producing fields will reach the end of their lives. There has been a large production in subsea pipelines since 2003 [2]. These pipelines will eventually be decommissioned, and this will potentially lead to increased market demand for PRT's in the near future. There are many different solutions available in the market used for subsea pipeline recovery. An example of a PRT is presented in Figure 1. PRTs often use a mechanical system to insert/wrap over and lock itself to the subsea pipeline.

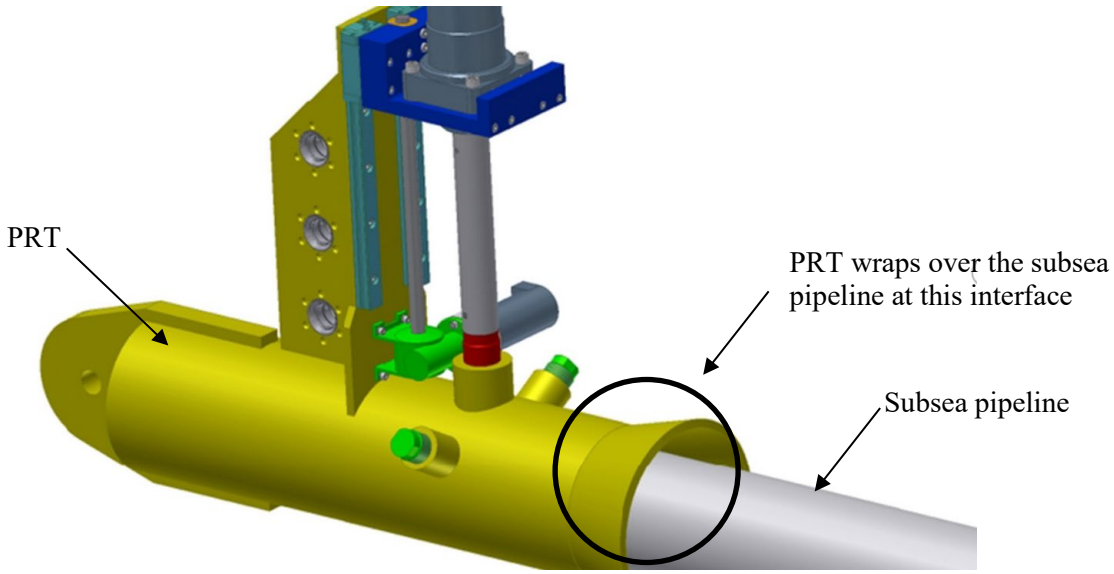

Figure 1. IK-Norway pipeline recovery tool, Ref. IK-Norway [3].

A unique wedge-lock and sealing technology that utilizes steel balls casted in polyurethane (PUR) is presented in this paper. The steel balls form a ball-grip mechanism together with a cone and presses steel balls against the inner diameter of the subsea pipeline to generate large contact stress. This in turns locks the PRT onto the subsea pipeline. The polyurethane presses itself on the inner diameter of the pipeline and this forms a sealing mechanism sealing off the pipeline during the recovery operation. This sealing mechanism that has its origins from IK-Norway's plug technology. Details of the prototype PRT and its unique wedge-lock and sealing technology is presented in Section 3. The ability to seal the subsea pipeline allows the pipeline to be flushed before retrieval. This leads to reduction in operational costs.

This paper studies the contact stresses associated the wedge-lock mechanism using numerical and physical testing methods. The purpose is to characterize the design of the wedge-lock mechanism. This paper presents the first stage of the study in which the sealing mechanism is not studied. This means that the steel balls without the PUR is modelled and physically tested. There are plans to study the steel balls casted in PUR in the second stage of the study in the near future.

2. Subsea pipeline recovery operation

The subsea pipeline recovery operation is briefly described in this section. The operation typically follows the steps below:

- The PRT is inserted at the end of the subsea pipeline using a remotely-operated vehicle.
- A hydraulic load is applied to the PRT to activate the locking mechanism. At this stage, the PRT is locked onto the subsea pipeline.
- The PRT is then pulled up to the surface thereby recovering the subsea pipeline.

The PRT can grip the pipeline on the inner or outer diameter. In the case where the PRT grips the pipeline on its outer diameter i.e., the PRT would warp over the pipeline as illustrated in Figure 1,.

3. Prototype pipeline recovery tool (PRT)

The prototype PRT is presented in Figure 2. This tool is designed to recover a 12-inch subsea pipeline. It is designed to recover pipelines manufactured in accordance with the ASME B36.10M [4] dimensions. Item number 8 in Figure 2 is a bearing steel ball embedded in polyurethane (PUR). Illustrative details of this can be found in Figure 4.

Part List	
Item	**Title**
1	Main Body PRT
2	Set-Force Body
3	PUR-Pipeline Packer
4	PUR-sealing packer with bearing steel balls
5	ROV-Handle
6	Two-Way Cylinder
7	Studbolt
8	Bearing Steel Ball

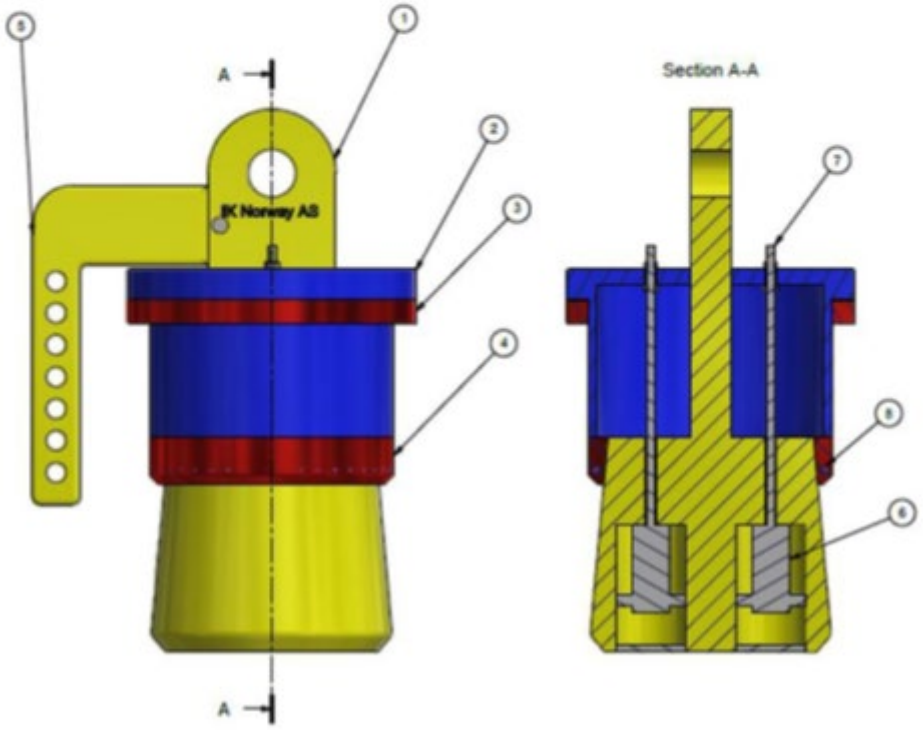

Figure 2. Prototype pipeline recovery tool.

3.1. The wedge-lock and sealing mechanism

The mechanism functions in the following manner as illustrated in Figure 3:

- The tool is inserted into one end of the subsea pipeline; Step 1 in Figure 3
- The cone is pulled towards the force-set pipe using hydraulics. This causes the force-set pipe to press onto the polyurethane (PUR); Step 2 in Figure 3
- The PUR then presses onto the steel balls (casted in the PUR); Step 3 in Figure 3
- The steel balls press onto the cone and the pipeline. This generates the large contact stresses and therefore the gripping force required to lock the PRT to the pipeline.
- The PUR also presses against the cone and pipeline. This seals the pipeline with the PRT.
- The PRT can now pull the pipeline; Step 4 in Figure 3

The above steps are also illustrated in Figure 3. An illustration of the wedge-lock and sealing mechanism is presented in Figure 4.

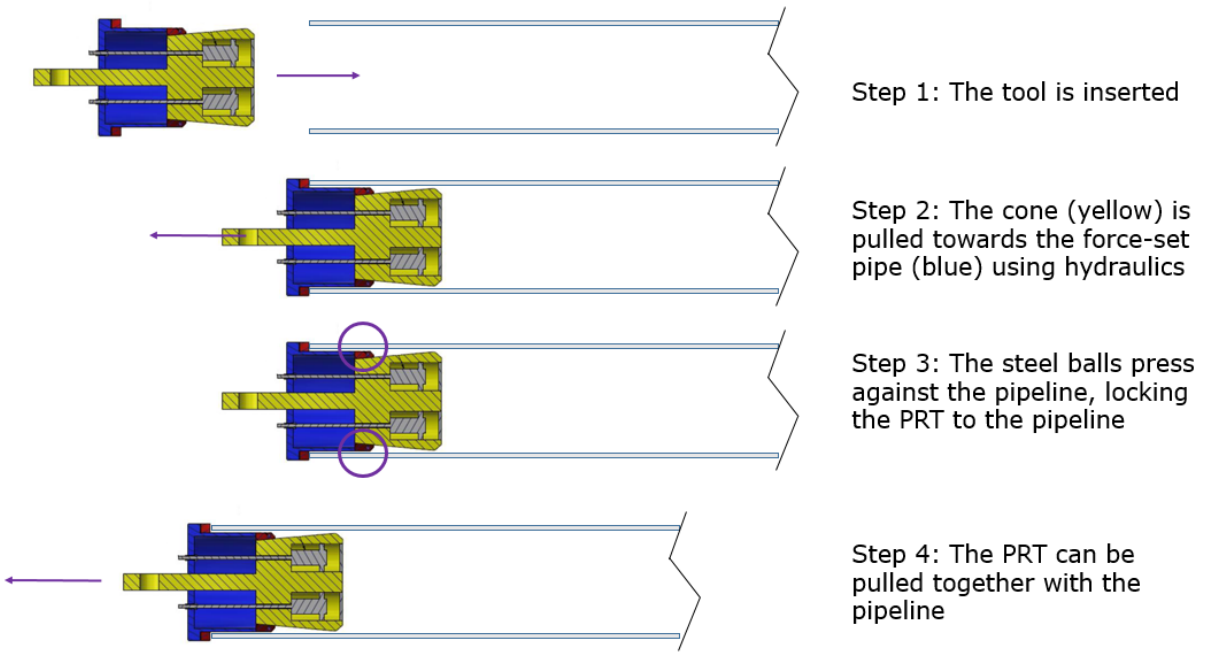

Figure 3. Step-by-step illustration of the PRT in use.

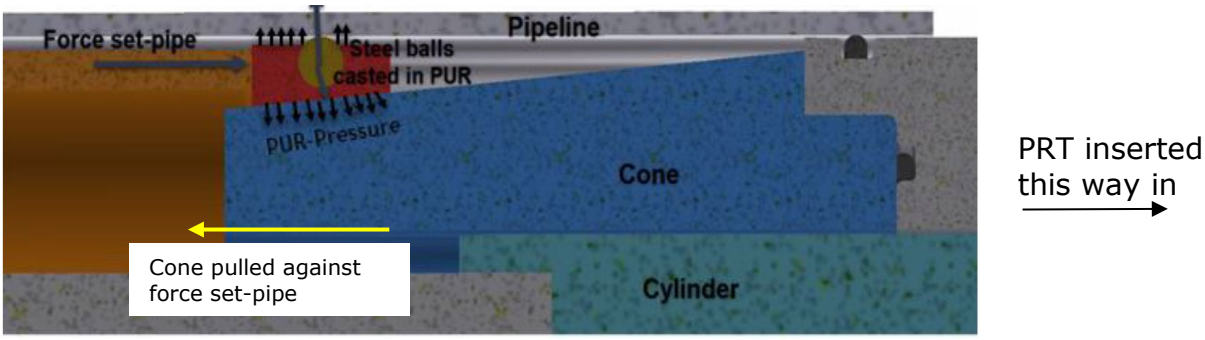

Figure 4. Wedge-lock and sealing mechanism.

4. Finite element modelling

The load and stress patterns are symmetrical about the mid-plane of the steel ball therefore a 1/32 model is used; there are a total of 32 steel balls.

4.1. FE model details

This section presents the FE model details.

4.1.1. Loads and boundary conditions. The loads and boundary conditions applied on the model are illustrated in Figure 5. Note that frictionless support is applied at all out-of-plane surfaces to take into account of the symmetrical condition about the middle of the steel ball. A 3D view of the model showing the loads and boundary conditions is presented in Figure 6.

4.1.2. Material model. A bilinear material curve is used in the FE model for the pipeline. The material properties are taken from the properties for S355 steels in DNVGL-RP-C208 [5]. The elastic modulus is 210 000 Mpa and the yield strength is 335 MPa. The cone and steel ball are modelled as elastic material with elastic modulus of 210 000 MPa. The cone and steel ball are prescribed to be high strength

steel with much higher yield strength than the pipeline. They are not meant to plastically deform in real life.

4.1.3. Mesh details. The mesh details are presented in Figure 5. The contact element size used is 0.2 mm. There are a total of 162 960 10-node tetrahedral elements with 236 880 nodes. The mesh size is determined via a mesh refinement study presented in Section 4.2.

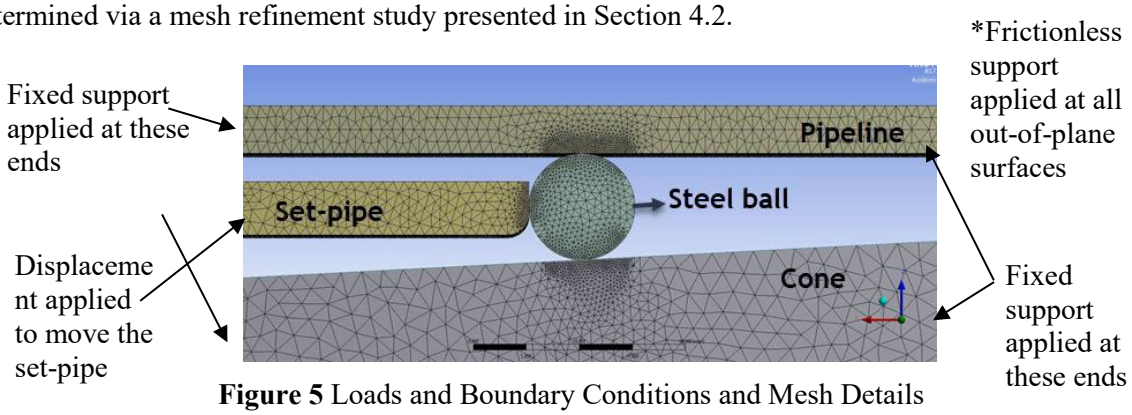

Figure 5 Loads and Boundary Conditions and Mesh Details

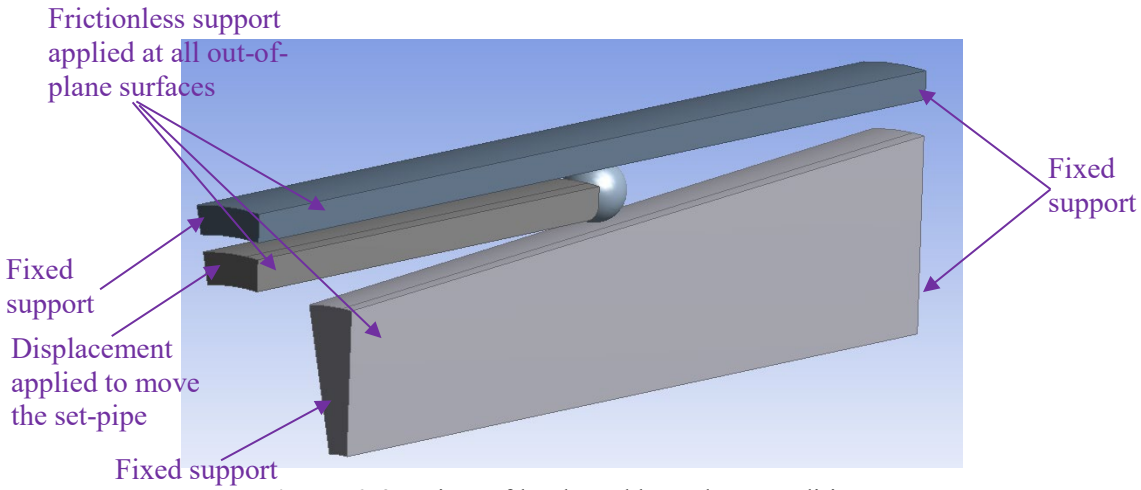

Figure 6. 3D view of loads and boundary conditions.

4.2. Mesh refinement study

A mesh refinement study focusing on the contact area with the following cases as presented in Table 1 investigated. A mesh refinement study was not performed for the other parts of the model. In these parts, there are at least five layers of elements in any given direction for these parts. This is considered to be sufficiently fine.

Table 1. Cases studied for mesh refinement study.

Contact element size (mm)	No. of elements	No. of nodes
0.15	337 523	478 814
0.2	162 960	236 880
0.3	73 879	112 109
0.4	51 437	79 632
0.5	42 879	67 229

The results of the mesh refinement study are presented in Figure 7 and show that a contact element sizing of 0.2 mm produces sufficiently converged results. Therefore this is used in the paper.

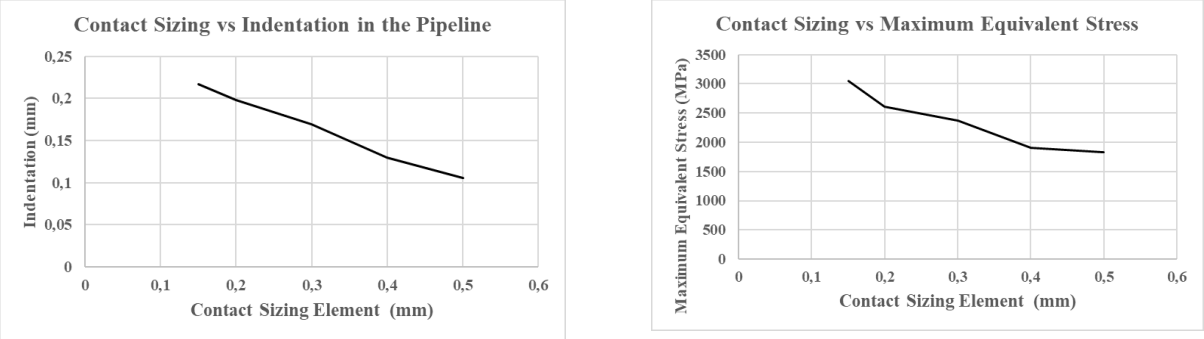

Figure 7. Results of mesh refinement study.

4.3. Example results

Some example result plots are presented in Figure 8 and Figure 9. Figure 8 shows the von Mises stress patterns.

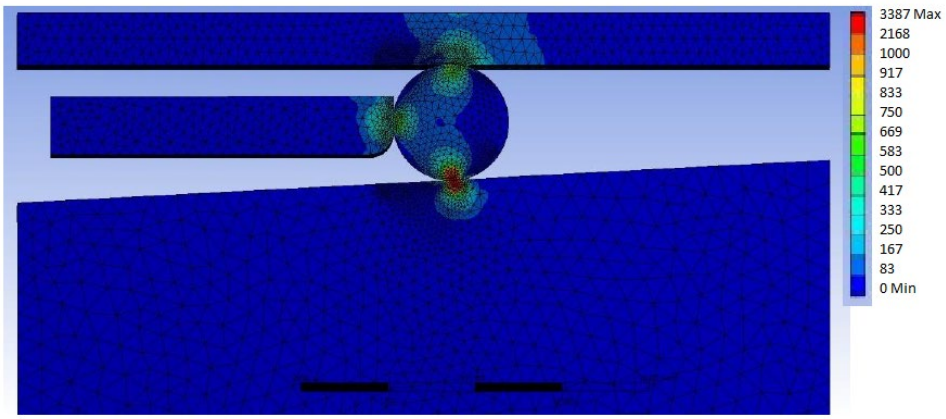

Figure 8. Von-Mises stresses pattern.

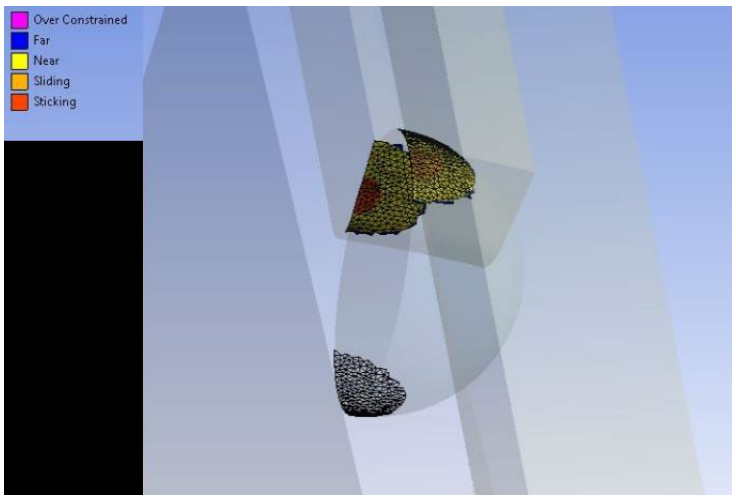

Figure 9. Overview of sticking/sliding status at the steel ball.

5. Experimental test set-up

A test rig was fabricated to model the wedge-lock and sealing mechanism. The cross-sectional view of the test rig is presented in Figure 10. In this test rig, the set-pipe is pushed towards the cone using a hydraulic press as presented in Figure 11. This is in the opposite direction of what will occur in the actual design where the set-pipe is pulled towards cone. However, the physical stresses/forces generated are the same for both cases. Note that Figure 10 shows the polyurethane part. In the actual tests, the steel balls were tested without the polyurethane part, i.e., only the wedge-lock mechanism is investigated.

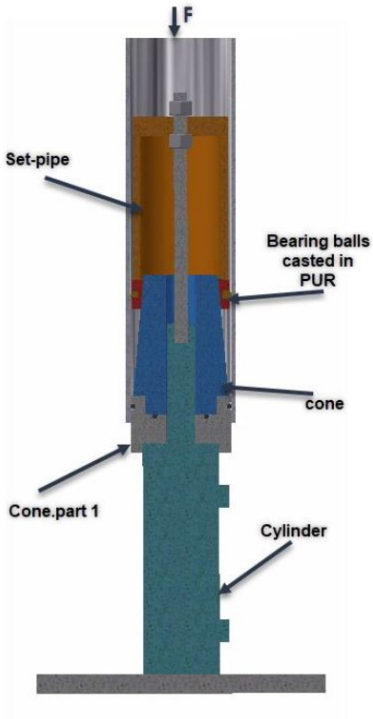

Figure 10. Cross-sectional view of test jig

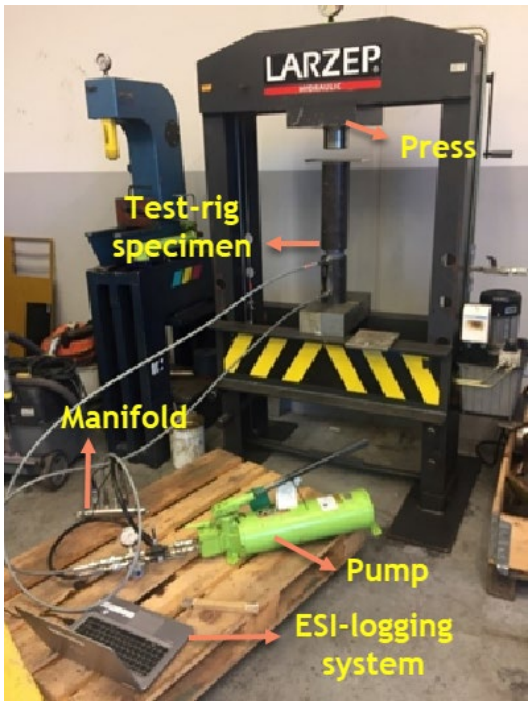

Figure 11. Test jig on the hydraulic press.

5.1. Test rig components

The components in the test rig and their corresponding numbering are presented in Table 2 and Figure 12, respectively.

Table 2. Components used in test rig.

Part number	Component	Comment
1	Steel ball	Ref. Section 5.1.1.
2	Cone part 2	Ref. Section 5.1.2.
3	Pipe	Ref. Section 5.1.3.
4	Cone part 1	Ref. Section 5.1.2.
5	Set-pipe	Ref. Section 5.1.4.
6	Polyurethane	Not tested

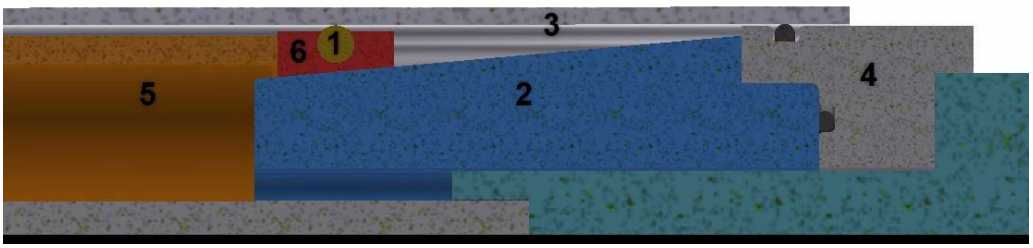

Figure 12. Numbering of components in test rig.

5.1.1. Steel ball. The steel balls used have a diameter of 10 mm and are made in accordance with the standard DIN 17230 [5] and have a hardness of at least 740 HV10, which is between 57 and 58 HRC. There are a total of 32 steel balls in the test rig.

5.1.2. Cone. The cone consist of two parts, part 1 and part 2. Part 2 is the part that presses against the steel balls. Part 1 is an interfacing component that is used to hold Part 2 in place. A total of six cones as presented in Figure 13 were manufactured. However, only the 3 °cone were completely tested in the test. The definition of the cone angle is presented in Figure 14. The cones are made from Uddeholm Calmax steel for high toughness, high wear resistance and high through hardening properties [7].

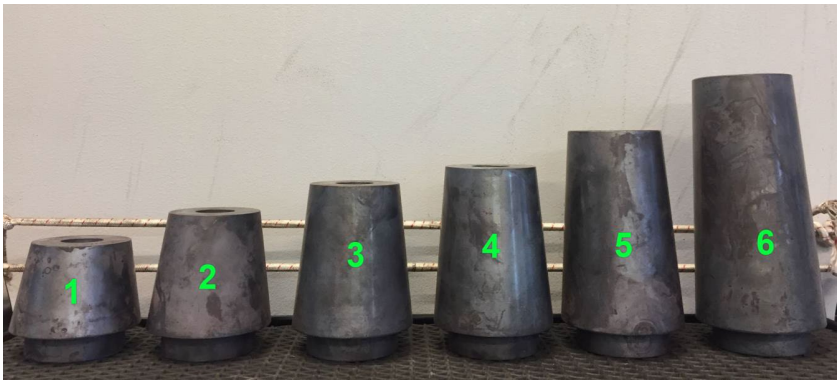

Figure 13. Six cones (part 2) with angles of 10°, 8°, 6°, 5°, 4° and 3° were manufactured. However, only the cone with 3°angle was completely tested in the test.

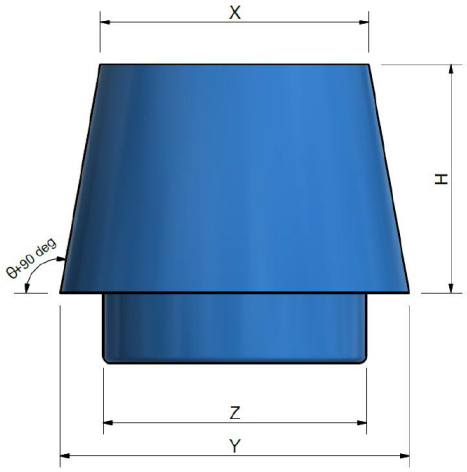

Figure 14. Definition of cone angle, θ

5.1.3. Pipe. The pipe is a steel tube with a tensile strength of 450 MPa and a yield strength of 388 MPa at the measured section. This is the component with the lowest yield strength that is in contact with the steel balls.

5.1.4. Set-pipe. This is a machined pipe. A hydraulic press is used to press this against the cone and pipe.

5.2. Indentation at test components
Figure 15 and Figure 16 show the indentations observed at the test components after the physical tests.

Figure 15. Indentation at the pipe and cone.

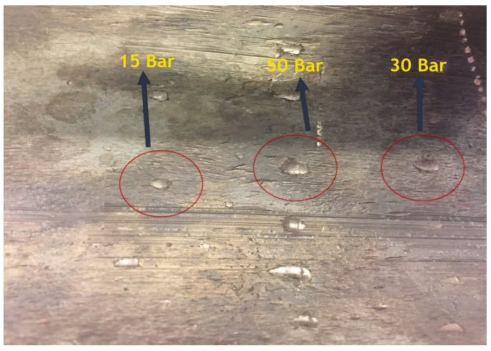

Figure 16. Zoom-in at indentation at the pipe

6. Results and discussions

6.1. FE results and discussions
The results from the linear-elastic and elastic-plastic model shows that friction coefficient has a major impact on reaction force, equivalent stress and indentation depth. This can be observed from the results presented in Figure 17 and Figure 18. Another parameter that affects the results significantly is yield stress of the pipe. This is shown in Figure 19.

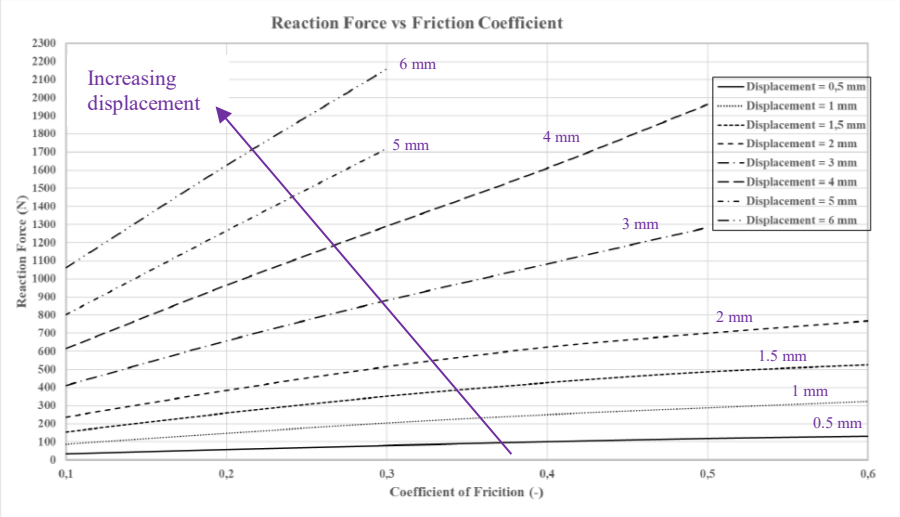

Figure 17. Reaction force vs. friction coefficient, FE model tesults, 3° cone.

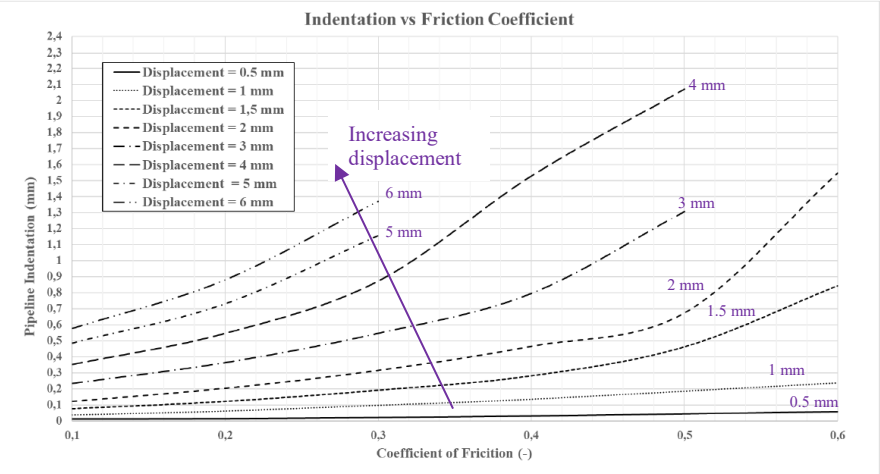

Figure 18. Indentation vs. friction coefficient, FE model results, 3° cone

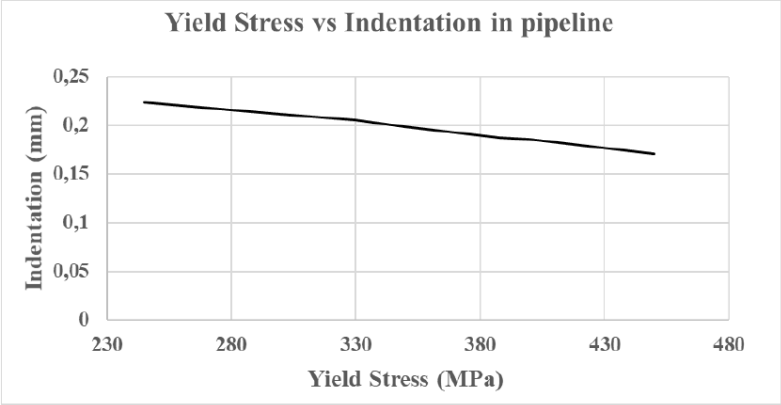

Figure 19. Indentation vs. yield stress, FE model results, 3° cone

6.2. Physical testing results and discussions

The displacement of the steel balls caused by the applied force from the set-pipe causes the steel balls to deform both cone and steel pipe as shown in Figure 15 and Figure 16. As expected, the results as presented in Figure 20 show that there is a correlation between the angle of the cone, set-pressure and indentation. The figure shows that indentation has an approximately linear relationship with the set-pressure. However, the results with the cone-angle of 4 ° does not have the same slope on the results as the other cone-angles. This implies that there are irregularities in these results. A possible explanation is that the cone is misaligned during the test.

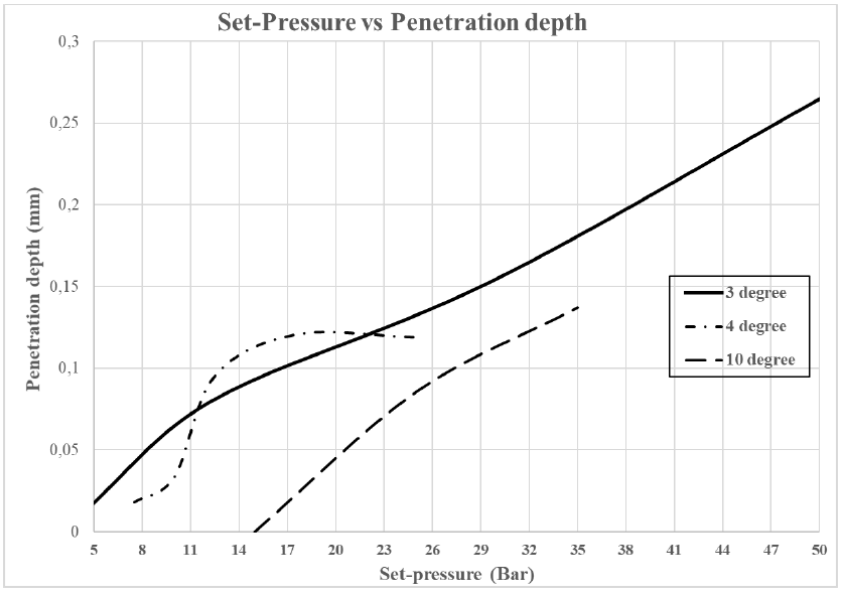

Figure 20. Indentation depth vs set-pressure, physical testing.

6.3. Comparison between FE model and physical test results

The comparison between the FE model and physical test results is presented in Table 3. The table is read in the following manner:

- The indentation depth is measured from the physical tests and corresponds to a given set-pressure. In this case, three set-pressures of 10, 15 and 30 bar were investigated.
- The set-pressure is converted to the corresponding reaction force and displacement at the set-pipe and the corresponding friction coefficient range is read from the FE model results as presented in Figure 17, Figure 18 and Figure 19.

The results compare well for a certain range of friction coefficients which in fact corresponds to the typical range of friction coefficients founds in engineering application for lubricated metal surfaces.

Table 3. Comparison between FE model and physical test results, 3° cone.

Set-pressure – physical test (bar)	Indentation depth – physical test (mm)	Friction coefficient range – FE model
30	0.18	0.15 to 0.3
15	0.085	0.1 to 0.4
10	0.06	0.15 to 0.4

7. Conclusions

The following conclusions are made:

- The size and simplicity of the prototype PRT suggests savings in maintenance and operations can be made.
- Uncertainties in the coefficient of friction and yield stress lead to significant variations in the results.
- The FE model gives a good representation of the test-rig if the friction coefficient is known.
- A low friction coefficient ensures a minimum indentation depth. Low friction coefficients can be achieved by lubricating the steel balls.
- The results show that an increase in the cone-angle will lead to a decrease in the indentation depth when the same magnitude of force is applied on the steel balls.

8. Future Work

The sealing mechanism of the PRT is planned to be studied in future work. The planned approach is to investigate the sealing capacity of the polyurethane using numerical modelling and experimental tests. Polyurethane is a polymer which can be very sensitive to input conditions such as strain rates and temperature and therefore requires special considerations.

Acknowledgments

The authors would like to express thanks to IK-Norway for the support in the financing of the test rig and providing the facilities for the experimental testing.

References

[1] Manoucherhri, S., Subsea Pipelines and Flowlines Decomissioning – What We Should Know for a Rational Approach, Paper No. OMAE2017-61239, Proceedings of ASME 2017 36th Internal Conference on Ocean, Offshore and Arctic Engineering, Trondheim, Norway, 2017
[2] Venas, A., Offshore Pipelines Outlook, DNVGL Report, 2016
[3] IK-Norway, Special Design, Lifting Tools, Retrieved 18.07.2019 from https://ik-worldwide.com/product/products-and-services/subsea/studies/consept-selection/special-design-lifting-tools/
[4] ASME B36.10M -2018 Welded and Seamless Wrought Steel Pipe
[5] DNVGL-RP-C208, Determination of Structural Capacity by Non-Linear FE Analysis Methods, 2013
[6] DIN 17230 Beall and Roller Bearing Steels – Technical Condition of Delivery, 1980
[7] Uddeholm Calmax, Assab, Retrieved 18.07.2019 from http://www.assab-singapore.com/media/CALMAX-D20140711.pdf